



Combination of vinblastine and oncolytic herpes simplex virus vector expressing IL-12 therapy increases antitumor and antiangiogenic effects in prostate cancer models

Citation

Passer, Brent J., Tooba Cheema, Shulin Wu, Chen-lee Wu, Samuel D. Rabkin, and Robert L. Martuza. 2013. "Combination of vinblastine and oncolytic herpes simplex virus vector expressing IL-12 therapy increases antitumor and antiangiogenic effects in prostate cancer models." *Cancer gene therapy* 20 (1): 10.1038/cgt.2012.75. doi:10.1038/cgt.2012.75. <http://dx.doi.org/10.1038/cgt.2012.75>.

Published Version

doi:10.1038/cgt.2012.75

Permanent link

<http://nrs.harvard.edu/urn-3:HUL.InstRepos:11878913>

Terms of Use

This article was downloaded from Harvard University's DASH repository, and is made available under the terms and conditions applicable to Other Posted Material, as set forth at <http://nrs.harvard.edu/urn-3:HUL.InstRepos:dash.current.terms-of-use#LAA>

Share Your Story

The Harvard community has made this article openly available.
Please share how this access benefits you. [Submit a story](#).

[Accessibility](#)



Published in final edited form as:

Cancer Gene Ther. 2013 January ; 20(1): . doi:10.1038/cgt.2012.75.

Combination of vinblastine and oncolytic herpes simplex virus vector expressing IL-12 therapy increases antitumor and antiangiogenic effects in prostate cancer models

Brent J. Passer, Tooba Cheema, Shulin Wu[†], Chen-lee Wu[†], Samuel D. Rabkin, and Robert L. Martuza

[†]Departments of Neurosurgery and Pathology Massachusetts General Hospital and Harvard Medical School.

Abstract

Oncolytic herpes simplex virus-1 (oHSV)-based vectors selectively replicate in tumor cells causing direct killing, ie., oncolysis, while sparing normal cells. oHSV's are promising anticancer agents, but their efficacy, when used as single agents, leaves room for improvement. We hypothesized that combining the direct oncolytic and antiangiogenic activities of the IL-12 secreting NV1042 oHSV with microtubule disrupting agents (MDA's) would be an effective means to enhance antitumor efficacy. Vinblastine (VB) was identified among several MDA's screened that displayed consistent and potent cytotoxic killing of both prostate cancer and endothelial cell lines. In matrigel tube forming assays, VB was found to be highly effective at inhibiting tube formation of HUVEC cells. The combination of VB with NV1023 (the parental virus lacking IL-12) or NV1042 showed additive or synergistic activity against prostate cancer cell lines and was not due to increased oHSV replication by VB. In athymic mice bearing CWR22 prostate tumors, VB in combination with NV1042 was superior to the combination of VB plus NV1023 in reducing tumor burden, appeared to be nontoxic and resulted in a statistically significant diminution in the number of CD31⁺ cells as compared to other treatment groups. In human organotypic cultures using surgical samples from radical prostatectomies, both NV1023 and NV1042 were localized specifically to the epithelial cells of prostatic glands but not to the surrounding stroma. These data highlight the therapeutic advantage of combining the dual-acting anti-tumor and anti-angiogenic activities of oHSV's and MDA's.

Keywords

oncolytic HSV-1; prostate cancer; IL-12; angiogenesis; microtubule disrupting agents; combination therapy

Introduction

Selectively replication-competent viral vectors, such as oncolytic herpes simplex viruses type 1 (oHSVs) are genetically engineered from herpes-simplex virus (HSV) type I. These lytic viruses represent an attractive strategy for tumor-based therapies because they can specifically replicate and spread in cancer cells *in situ*, exhibiting oncolytic activity through direct cytopathic effects while sparing normal cells. Since the first report of a conditionally

replicating genetically engineered virus¹, a number of oHSV vectors have been developed which are highly effective against a myriad of solid tumors²⁻⁵. For example, NV1023 and the IL-12 expressing NV1042, are derived from an HSV1/2 intertypic mutant, which retains one copy of gamma34.5 gene⁶. NV1042 has been shown to inhibit squamous cell carcinoma growth through both antiangiogenic mechanisms as well as direct cytopathic effects⁷. We have shown that NV1042 is superior to the NV1023 parent vector in inhibiting prostate cancer growth of both primary and metastatic tumors via both immune and antiangiogenic mechanisms in syngeneic mouse models⁸⁻¹⁰. The antiangiogenic activity is due, in part, to the induction of IFN γ pro-inflammatory activities¹¹. IFN γ affects the neovasculature through induction of the angiostatic chemokines CXCL9 (MIG) and CXCL10 (IP-10), up-regulation of VCAM-1 and inhibition of MMP9 expression¹². Although IL-12 is also known to enhance antitumor response by inducing a Th1 response, it has also been shown that blood vessel formation is markedly decreased by IL-12 treatment in severe-combined immunodeficient (SCID) mice¹¹, suggesting that the antiangiogenic effects of IL-12 is independent of T and B-cells.

Previously, we reported that the combination of oHSV plus a microtubule disrupting agent (MDA), ie., docetaxel or paclitaxel, acts synergistically to promote prostate cancer cell killing *in vitro* and *in vivo*¹³. Similar synergistic interactions have been reported for another HSV-1 mutant as well as for vaccinia virus and reovirus in various cancers including prostate cancer¹⁴⁻¹⁶. In addition, studies involving the use of adenovirus mutants in combination with either paclitaxel or docetaxel have reported synergistic interactions in prostate cancer cells^{17,18}. MDA's have been shown to be effective inhibitors not only of tumor growth but also angiogenesis in numerous *in vivo* models¹⁹. In order to take additional advantage of a dual killing mechanism (tumor cells plus tumor endothelial cells) and to further improve upon the efficacy of currently available oncolytic vectors, we examined the strategy of using an "armed" oHSV expressing IL-12 combined with an MDA. We have evaluated the preclinical therapeutic effects of NV1042 (expressing IL-12) in combination with vinblastine and show that this combination enhances antitumor efficacy, in part by, inhibiting angiogenesis.

Materials and methods

Cells and viruses

Vero (African green monkey kidney), MS1 (mouse pancreatic endothelial), C166 (mouse yolk sac endothelial), CWR22 (human prostate cancer) and PC3 (human prostate cancer) cells were obtained from American Type Culture Collection (Manassas, VA) and human umbilical endothelial cells (HUVEC) from Lonza (Hopkinton, MA). HBME-1 (human bone marrow endothelial) cells were a generous gift from Dr. K. Pienta (University of Michigan). Vero cells were grown in DMEM supplemented with 10% calf serum and HUVEC in EGM-2. PC3 cells were grown in FK-1 media containing 10% heat-inactivated fetal calf serum (Hyclone, Logan, UT). Primary human prostate epithelial cells and its culture medium PrEGM were maintained as described by the manufacturer (Lonza). Construction of NV1023 and NV1042 has previously been described²⁰. NV1023, derived from NV1020 (R7020), a HSV-1/HSV-2 intertypic recombinant developed as a vaccine strain²¹, contains an insertion of *LacZ* into the *ICP47* locus, deleting *ICP47*, *US11*, and *US10*²⁰. NV1042 is NV1023 with an insertion of murine IL-12 cDNA (p35 and p40 as a single polypeptide separated by elastin motifs) expressed from a hybrid γ 4-TK promoter²⁰.

Cell Viability assays

Viability assays were performed over a 3 day period using the MTS assay kit (Promega, Madison, WI) in a 96-well format. The compounds used in this study included, Paclitaxel

(Bristol-Myers Squibb, Princeton, NJ), docetaxel (Aventis Pharmaceuticals Inc., Bridgewater, NJ), vinblastine (APP Pharmaceuticals, Schaumburg, IL), epothilone-B (EpoB) (Sigma-Aldrich), vincristine (Hospira Inc, Lake Forest, IL) and 2-methoxyestradiol (2ME2) (Sigma-Aldrich).

Virus titration

Monolayer cultures of Vero cells grown in a six-well plate were infected with serial dilutions of virus. After removal of virus inoculum, the cells were incubated in DMEM supplemented with 1% inactivated FCS and 0.1% pooled human immunoglobulin at 37°C for 3-4 days until plaques were visible and counted.

Virus Replication assay

Cells were seeded in 12-well plate 1 day before infection and infected with NV1023 or NV1042 at a multiplicity of infection (MOI) of 1. At the times indicated, cells were harvested from the wells and viral titers were determined on Vero cells. Prostate cancer and endothelial cell lines either remained untreated or were pretreated with vinblastine (0.1nM) for 12h and thereafter, cells were infected with NV1023 or NV1042 at an MOI of 1.5. At 24 or 48h after infection, cells were scraped into the medium and subjected to three freeze-thaw cycles. Virus titers were determined by plaque assays on Vero cells. Each concentration in an experiment was plated in duplicate, and each experiment was performed three times. Supernatants collected from single burst assays were assayed for IL-12 derived from NV1042 at the indicated time points by ELISA (R&D Systems, Minneapolis, MN) and normal goat IgG (2 µg/ml/well) (R&D Systems) was included as a species-specific control.

Cell susceptibility assays and Chou–Talalay analysis

Prostate cancer (PC3 and CWr22) and endothelial (HUVEC, HBM-1, C166 and MS1) cells were seeded into 96-well plates at 1500-3000 cells per well. Viability assays will be performed over a 3 day period using the MTS assay kit (Promega) with a concentration range of MDA's and varying MOI's of oHSV. Dose-response curves were generated using GraphPad v5.0 (San Diego, CA). For Chou–Talalay analysis, dose–response curves and 50% effective dose values (ED₅₀) were obtained and compared at day 3. For ED₅₀ determination, cells were incubated for 3 days with varying concentrations or MOIs of drug and virus, respectively, and cell survival was then assessed using MTS assays. Dose–response curves were fit to Chou–Talalay lines, which are derived from the law of mass action and are described by the equation $\log(f_a/f_u) = m \log D - m \log D_m$, in which f_a is the fraction affected (percent cell death), f_u is the fraction unaffected (percent cell survival), D is the dose, D_m is the median-effect dose (the dose causing 50% of cells to be affected, that is, 50% survival), and m is the coefficient signifying the shape of the dose–response curve. The combination index (CI)-isobologram by Chou and Talalay²² was used to analyze virus and drug combinations. Fixed ratios of virus and drug concentrations and mutually exclusive equations were used to determine CIs. All experiments were repeated at least three times.

Tube formation assay

HUVEC cells (~90,000 cells/well) were added to Matrigel™ (BD Biosciences) -coated 24-well plates. Four hours later, docetaxel (10nM), vinblastine (10 nM), vincristine (10nM), EpoB (10 µM) or 2ME2 (10 µM) were added in triplicate. For combination studies, NV1023 or NV1042 (MOI 1) with or without vinblastine (1 nM) were added. Twenty hours later tube formation was quantified by counting the branching points for each well by light microscopy.

In vivo studies

CWr22 cells (5×10^6 cells) were implanted subcutaneously into the flanks of 6-to 8-week-old balb/c *nu/nu* mice ($n=8$ mice per group). When the tumor volume reached 75-150 mm^3 (~14 days after implantation) mice were stratified by tumor volume and then randomly assigned to treatment groups ($n=8$ per group). Virus [NV1023 or NV1042; 5×10^5 plaque-forming units (pfu)] or virus suspension buffer (PBS with 10% glycerol) was injected intratumorally on days 13 and 15 after tumor implantation. Vinblastine monotherapy or its combination with virus was administered intraperitoneally on day 15 at 0.35 mg/kg for nine consecutive days. All procedures were approved by the MGH Subcommittee on Research Animal Care. Tumor volume was calculated using the formula width (mm)² \times length (mm) \times 0.52.

CD31 immunohistochemistry and quantification

Mice ($n=3$ /group) were treated as described above and at day 30 post-implantation tumors were harvested, frozen and cut into tissue sections. Tissue sections were stained with a rat anti-mouse CD31 antibody (BD Biosciences, San Jose, CA) followed by secondary anti-rat IgG conjugated to HRP (GE Healthcare, Piscataway, NJ). CD31⁺ staining was revealed with 3,3'-diaminobenzidine (DAB) histochemistry (Vector Laboratories, Burlingame, CA). Sections were counterstained with hematoxylin (Sigma, St. Louis, MO). Tumor microvessel density was quantified for all treatment groups. At least 6-10 representative 40X fields per view were captured as epifluorescent digital images using a Spot digital camera (Spot Diagnostic instruments, Sterling, MI). To calculate microvessel density, area occupied by CD31-positive microvessels and total tissue area, per section were quantified using Image J software (NIH, Bethesda, MD). Microvessel density was then calculated as a percentage of CD31 stained per tumor section.

Prostate organ cultures

Prostate organ cultures were performed as previously described²³. Briefly, tissue fragments were incubated with NV1023 (1×10^6 pfu) or NV1042 (1×10^6 pfu) for 1 h in direct contact and thereafter, placed on a semi-submersed collagen sponge (Ultrafoam™, Davol Inc., Warwick, RI) for 3 days. Tissue specimens (8 \times 8 mm) were stained with anti-HSV-1 gC (Virusys Corp., Sykesville, MD, USA) or anti-cytokeratin-8/18 (UCD/PR-10.11, Dakocytomation, Carpinteria, CA, USA) antibodies as previously described. Virus titers were determined by titration of tissue homogenates on Vero cells using plaque assays. Tissues weights were determined to correct for viral titer concentrations. (Average \pm S.E.M). Each color dot indicates a different prostate surgical specimen that was separately infected with either NV1023 or NV1042 ($n=5$).

Statistical analysis

All statistical analyses were done using GraphPad prism v5. For comparison of efficacy and mechanism of efficacy, unpaired Student's *t* test (two tailed) was used to analyze significance between two treatment groups.

Results

Evaluation of a panel of MDA's on endothelial and prostate cancer cell lines

MDA's have been shown to have broad-based antitumor and antiangiogenic properties^{19,24}. We initially screened a series of MDA's (docetaxel, paclitaxel, vinblastine, vincristine, epothilone-B and methoxyestradiol) on a panel of human (HUVEC, HBME1) and mouse- (MS1 and C166) derived endothelial and human prostate cancer cell lines. While the majority of MDA's tested yielded potent cytotoxic effects on all four endothelial cell lines,

vinblastine (VB), was consistently superior (EC_{50} = 0.18-1.7 nM), demonstrating potent dose-dependent endothelial cell killing (Figure 1A; Table 1). *In vitro* matrigel assays, which partially recapitulate the mechanisms of neovascularization observed *in vivo*, confirmed that VB was highly effective at inhibiting tube formation of HUVEC cells (Supplementary Figure 1). Furthermore, in prostate cancer cell lines, VB was more or equally potent as the other MDA's tested. For example, in the androgen-dependent CWR22 cell line, the cytotoxic effects of VB paralleled vincristine, while VB's cytotoxic effects on the androgen-independent PC3 cell line was similar to vincristine, docetaxel and paclitaxel (Figure 1B; Table 1). In contrast, EpoB and 2-ME2 had negligible effects on both endothelial and tumor cell lines. Lastly, when endothelial (HUVEC and HBME) or prostate cancer cells (CWR22 and PC3) were treated with MDA's for only 3 hrs and then washed away, VB was still cytotoxic, suggesting that even transient exposure of VB is effective (Supplemental Figure 2).

***In vitro* assessment of oHSV and MDA combination**

Previously, we reported that NV1023 and IL-12 secreting NV1042 were effective *in vitro* and *in vivo* at killing mouse prostate cancer cells⁸⁻¹⁰. To evaluate the cellular permissiveness of the human CWR22 and PC3 cancer cell lines toward NV1023 and NV1042, we performed viral burst assays. Figure 2A shows that by 48 hrs, virus production in CWR22 cells peaked, resulting in a ~32-fold increase in viral titers over input virus. By 72 hrs, the generation of virus progeny had plateaued. In PC3 cells, NV1023 and NV1042 virus production steadily increased over a 72 hr time period, resulting in a ~22-fold enhancement over input virus. Dose-response curves reflected the above findings, with both NV1023 and NV1042 more cytopathic toward CWR22 [EC_{50} = 0.24; Multiplicity of infection (MOI)] than PC3 (EC_{50} = 0.85 MOI) cells (Figure 2B). In addition, VB treatment of PC3 (EC_{50} = 7.8 nM) and CWR22 (EC_{50} = 4.2 nM) resulted in a dose dependent response over a 3d period (Figure 2C). IL-12 secretion after NV1042 infection showed relatively high levels in both prostate cancer cell lines over a 72 period, even though differences in viral titers were observed between cell lines (Figure 2D). Lastly, both NV1023 and NV1042 (data not shown) can replicate to various degrees in the four aforementioned endothelial cell lines (Supplemental Figure 3).

We used the combination index (*CI*) method of Chou-Talalay²² to assess whether the parental virus NV1023 in conjunction with VB could promote CWR22 or PC3 cell killing in a synergistic manner. A *CI* value of less than 1 indicates synergism and *CI*>1 indicates antagonism. Mild synergism (*CI*~0.8) was observed when NV1023 or NV1042 (EC_{50} = 0.24 MOI) and VB (EC_{50} = 4.2 nM) were added together in CWR22 cells (Figure 3). We further explored whether the observed synergistic effect was dependent on the timing of drug administration. A similar synergistic effect (*CI*~0.8) was observed regardless of whether VB was added 12hr before or after treatment of NV1023 or NV1042 (Figure 3C). Lastly, docetaxel but not EpoB could be substituted for VB in combination with NV1023 or NV1042 resulting in mild synergy (Figure 3C). In PC3 cells, the combination of NV1023 or NV1042 (EC_{50} = 0.85 MOI) with VB (EC_{50} =7.8 nM) resulted in an additive effect regardless of the order of administration. We also addressed whether the observed synergistic effects were due to increased oHSV replication by VB. The addition of a nontoxic concentration of VB (0.1 nM) to NV1023 neither increased nor decreased viral titers as compared to NV1023 alone at 48 hr after infection in single-step growth curve assays (Figure 2E). Lastly, in matrigel tube formation assays, we observed that the combination of either NV1023 or NV1042 (MOI 0.2) with VB (1 nM) was significantly more effective at disrupting tube formation than any single agent alone (Figure 4).

Preclinical evaluation NV1023 or NV1042 with vinblastine in CWR22 xenografts

Next, we evaluated the *in vivo* antitumor efficacy of NV1023 or NV1042 in combination with VB in subcutaneous CWR22 tumors in athymic mice. Initially, doses of individual therapies were established to determine conditions resulting in tumor size reductions of 20-50% (data not shown). Mice were treated with either mock control, NV1023 or NV1042 (5×10^5 pfu) on days 13 and 15, and/or VB (0.35 mg/kg; for 9 consecutive days) starting on day 15 (Figure 5A). By 32 days after tumor implantation, a statistically significant decrease in tumor volume was observed between control (2356 ± 746) and all of the treatment groups ($P < 0.05$, *; $P < 0.01$, **) (Figure 5B). As compared with mock, treatment with NV1023 (1575 ± 552), NV1042 (1087 ± 254) and VB (1623 ± 611) resulted in a notable reduction in tumor size; whereas the combination of NV1023/VB (1143 ± 321) was superior to either therapy alone. Importantly, NV1042 plus VB (487 ± 175 , $P < 0.01$, ***), was significantly more effective than NV1023 plus VB or NV1042 alone. These combination therapies appeared to be nontoxic to mice as their body weight were not statistically different (Supplementary figure 4). As the combination of NV1042/VB appeared to be more efficacious than any of the other treatment groups in reducing tumor volume, we hypothesized that this might be due, in part, to the combined antiangiogenic contributions of IL-12 and VB. This was tested using anti-CD31 antibody staining, which marks endothelial cells, on CWR22 tumor tissue sections. This revealed a reduction in CD31⁺ cells in the NV1042 plus VB treatment group as compared to the other treatment groups (Figure 5C). A statistically significant reduction in the number of CD31⁺ cells was observed in tumors treated with NV1042 plus VB as compared to all of the other treatment groups ($P < 0.05$, **) (Figure 5D). In addition, statistically significant differences were also observed between NV1023 and NV1042 treatment groups ($P < 0.05$, *), which is consistent with a previous report demonstrating a reduction of CD31-positive cells in murine prostate tumors treated with NV1042⁸.

Lastly, we wished to confirm specificity in an additional model system representative of human prostate cancer. Recently, we reported the use of human prostate organ cultures using surgical specimens derived from radical prostatectomies to assess oHSV target specificity and replication competence²³. We exploited this system to address the target specificity and replication competence of NV1023 and NV1042. At 3 days after infection, anti-HSV gC staining revealed that both NV1023 and NV1042 appeared to preferentially localize to the prostatic glandular regions in primary human prostate cancer tissues (Figure 6A). The staining of serial sections with anti-cytokeratin 8/18 antibody, which specifically stains luminal epithelial cells, confirmed that both vectors were restricted to epithelial cells and is in agreement with the restricted specificity of oHSV's previously seen in prostate cancer tissues²³. NV1023 and NV1042 replicated to similar degrees in five different prostate cancer tissue specimens examined (Figure 6B). Interestingly, the amount of replication for both viruses was similar in cultures from the same patient (same color dots, Fig 6B), as opposed to different patients.

Discussion

The discovery that tumors induce angiogenesis to generate new blood vessels for their growth and progression^{25,26} has recently led to numerous anti-angiogenic therapeutic strategies as well as demonstrated promise in improving the outcomes in cancer patients²⁷. Our study focused on implementing a treatment regimen for prostate cancer by combining the antitumor and antiangiogenic activities of an "armed" oncolytic oHSV (NV1042) with a cytotoxic microtubule disrupting agent, vinblastine, in order to improve antitumor efficacy. Of the six microtubule disrupting agents (MDA) tested, we found vinblastine to be the most potent at killing not only prostate cancer cells but also all endothelial cells. This is in

agreement with published observations that show that continuous treatment of VB at a low dose, can result in antiangiogenesis and sustained tumor regression²⁸.

Strategies of “arming” oHSV’s with anti-angiogenic transgenes have also shown promise in various preclinical models. For instance, IL-12 expressing NV1042 has shown enhanced therapeutic efficacy over NV1023 in subcutaneous or metastatic lung murine prostate cancer TRAMP-C2 tumors^{9,10} and C3(1)/T-Ag breast cancers²⁹. In addition, “armed” oHSV’s expressing other antiangiogenic agents such as dominant-negative fibroblast growth factor receptor, platelet factor-4 or angiostatin have been shown to substantially decrease blood vessel formation and increase survival³⁰⁻³².

In vivo, we demonstrate that the combination of IL-12 expressing NV1042 with low dose VB can enhance CWR22 tumor killing by partially impairing endothelial cell growth and/or neovascularization. VB alone administered at a low dose (0.35mg/kg) over a 9-day period, or NV1042 monotherapies were effective at promoting tumor regression. However, in combination a superior antitumor effect was observed, accompanied by minimal adverse side effects, such as stable body weight. The decreased tumor growth elicited by combining NV1042 with VB was most likely due to the cooperative effect on blood vessels as shown by the significant decrease in CD31+ blood vessels as well as the cytotoxic effects on tumor cells by either agent. Angiogenesis is a complex process that involves multiple regulatory proteins and endothelial cell activation. Endothelial cells that make up existing blood vessels are activated to multiply and migrate as surrounding basement membrane and extracellular matrix is degraded to make way for new capillaries. IL-12 primarily modulates tumor growth by the recruitment of immune cells such as natural killer cells and T cells³³. Our previous work addressed the antitumor and anti-angiogenic properties of the NV1042 expressing IL-12 virus in both syngeneic and transgenic mouse models of prostate cancer⁸⁻¹⁰. In this paper, our study focused on the anti-angiogenic effects of NV1042 in combination with vinblastine in human prostate cancers. Therefore, we utilized athymic xenograft models of prostate cancer, which lack T-cells and therefore, eliminates the tumor regression effects contributed by T-cells³⁴. However, nude and SCID mice have relatively normal levels of NK-cells, which have been shown to contribute, in part, to the inhibition of angiogenesis by IL-12^{11,35}. Our data show that NV1042 was superior to NV1023 either alone or in combination with vinblastine in slowing tumor growth in nude mice and that these results correlated with the percentage CD31+ blood vessels in tumor xenografts as a function of treatment condition.

Previous studies have shown that chemotherapy can enhance oncolytic viral replication³⁶. *In vitro*, we did not observe any significant change in NV1042/NV1023 viral yield in the presence of vinblastine. This is in accordance with our previous findings, where pretreatment with nontoxic concentrations of taxanes had negligible effects on G47 Δ replication¹³. A similar dose-range of either docetaxel or paclitaxel in combination with G47 Δ significantly increased prostate cancer cell killing¹³. In the present study, irrespective of treatment sequence with the combination of NV1023/NV1042 and VB, a weak synergy-to-additive effect was observed. Because Δ -herpesviruses are dependent on intact microtubules for efficient transport and egress³⁷, MDA treatment would be expected to compromise NV1023/NV1042 replication, particularly under conditions where vinblastine was added prior to virus infection. Disruption of microtubules by MDA’s such as nocodazole or taxol (ie., paclitaxel), have shown varying effects on HSV-1 transport and replication. Avitabile and colleagues reported that neither MDA significantly affected the release of free virus into the media at micromolar concentrations³⁸. In contrast, Kotaskis et al, reported that treatment of synchronized cells with nocodazole or taxol at similar concentrations prevented optimal HSV-1 replication³⁹. These discrepancies may be attributed to whether cells were synchronized or alternatively, due to differences in the

sensitivities of cells to nocodazole or taxol. A likely explanation for the observed weak synergy-to-additive effects is that at low VB concentrations, microtubules are minimally disrupted, which would allow for sufficient NV1023/NV1042 replication. In agreement these observations, the addition of G207 to nanomolar concentrations of paclitaxel resulted in weak synergy in promoting thyroid cancer cell killing with minimal effects G207 replication⁴⁰.

Combination therapy regimens with anti-angiogenic agents will be critical to treat prostate cancer, as microvessel density has been shown to correlate strongly with Gleason grade and predict disease progression^{41,42}. Although a recently concluded phase III trial of prostate cancer using bevacizumab (anti-VEGF antibody) in addition to the current standard of docetaxel and prednisone was negative⁴³ other antiangiogenic strategies are worth exploring and the use of dual angiogenesis inhibition with direct oncolytic oHSV therapy is an attractive strategy for prostate cancer, and can hopefully be used to overcome resistance that is observed with anti-angiogenic monotherapies⁴⁴.

Supplementary Material

Refer to Web version on PubMed Central for supplementary material.

Acknowledgments

We thank Melissa Marinelli for laboratory assistance. We also thank Dr. K. Pienta (University of Michigan) for the bone marrow-derived HBME-1 endothelial cells. The authors have no potential conflicts of interest.

Grant support: Support for this study was in part from a grant to RLM (R01CA102139).

References

1. Martuza RL, Mallick A, Markert JM, Ruffner KL, Coen DM. Science. 1991; 252:854–856. [PubMed: 1851332]
2. Mineta T, Rabkin SD, Yazaki T, Hunter WD, Martuza RL. Attenuated multi-mutated herpes simplex virus-1 for the treatment of malignant gliomas. Nat Med. 1995; 1:939–943.
3. Varghese S, Rabkin SD. Oncolytic herpes simplex virus vectors for cancer virotherapy. Cancer Gene Ther. 2002; 9:967–978. [PubMed: 12522436]
4. Kuruppu D, Tanabe KK. Viral oncolysis by herpes simplex virus and other viruses. Cancer Biol Ther. 2005; 4:524–531.
5. Kaur B, Chiocca EA, Cripe TP. Oncolytic HSV-1 Virotherapy: Clinical Experience and Opportunities for Progress. Curr Pharm Biotechnol. 2011
6. Wong RJ, Patel SG, Kim S, DeMatteo RP, Malhotra S, Bennett JJ, et al. Cytokine gene transfer enhances herpes oncolytic therapy in murine squamous cell carcinoma. Hum Gene Ther. 2001; 12:253–265. [PubMed: 11177562]
7. Wong RJ, Chan MK, Yu Z, Ghossein RA, Ngai I, Adusumilli PS, Stiles BM, Shah JP, Singh B, Fong Y. Angiogenesis inhibition by an oncolytic herpes virus expressing interleukin 12. Clin Cancer Res. 2004; 10:4509–4516. [PubMed: 15240543]
8. Varghese S, Rabkin SD, Liu R, Nielsen PG, Ipe T, Martuza. Enhanced therapeutic efficacy of IL-12, but not GM-CSF expressing oncolytic herpes simplex virus for transgenic mouse derived prostate cancers. Cancer Gene Ther. 2005; 13:253–265. [PubMed: 16179929]
9. Varghese S, Rabkin SD, Nielsen PG, Wang W, Martuza RL. Systemic oncolytic herpes virus therapy of poorly immunogenic prostate cancer metastatic to lung. Clin Cancer Res. 2006; 12:2919–2927. [PubMed: 16675589]
10. Varghese S, Rabkin SD, Nielsen GP, MacGarvey U, Liu R, Martuza RL. Systemic therapy of spontaneous prostate cancer in transgenic mice with oncolytic herpes simplex viruses. Cancer Res. 2007; 67:9371–9379. [PubMed: 17909046]

11. Duda DG, Sunamura M, Lozonchi L, Kodama T, Egawa S, Matsumoto G, Shimamura H, Shibuya K, Takeda K, Matsuno S. Direct in vitro evidence and in vivo analysis of the antiangiogenesis effects of interleukin 12. *Cancer Res.* 2000; 60:1111–1116. [PubMed: 10706132]
12. Mitola S, Strasly M, Prato M, Ghia P, Bussolino F. IL-12 regulates an endothelial cell-lymphocyte network: effect on metalloproteinase-9 production. *J Immunol.* 2003; 171:3725–3733. [PubMed: 14500672]
13. Passer BJ, Castelo-Branco P, Buhrman JS, Varghese S, Rabkin SD, Martuza RL. Oncolytic herpes simplex virus vectors and taxanes synergize to promote killing of prostate cancer cells. *Cancer Gene Ther.* 2009; 7:551–560. [PubMed: 19197321]
14. Lin SF, Gao SP, Price DL, Li S, Chou TC, Singh P, Huang YY, Fong Y, Wong RJ. Synergy of a herpetic oncolytic virus and paclitaxel for anaplastic thyroid cancer. *Clin Cancer Res.* 2008; 14:1519–1528. [PubMed: 18316577]
15. Huang B, Sikorski R, Kim DH, Thorne SH. Synergistic anti-tumor effects between oncolytic vaccinia virus and paclitaxel are mediated by the IFN response and HMGB1. *Gene Ther.* 2011; 18:164–172. [PubMed: 20739958]
16. Heinemann L, Simpson GR, Boxall A, Kottke T, Relph KL, Vile R, Melcher A, Prestwich R, Harrington KJ, Morgan R, Pandha HS. Synergistic effects of oncolytic reovirus and docetaxel chemotherapy in prostate cancer. *BMC Cancer.* 2011; 11:221. [PubMed: 21645351]
17. Radhakrishnan S, Miranda E, Ekblad M, Holford A, Pizarro MT, Lemoine NR, Hallden G. Efficacy of oncolytic mutants targeting pRb and p53 pathways is synergistically enhanced when combined with cytotoxic drugs in prostate cancer cells and tumor xenografts. *Hum Gene Ther.* 2010; 10:1311–1325. [PubMed: 20497039]
18. Oberg D, Yanover E, Adam V, Sweeney K, Costas C, Lemoine NR, Halldén G. Improved potency and selectivity of an oncolytic E1ACR2 and E1B19K deleted adenoviral mutant in prostate and pancreatic cancers. *Clin Cancer Res.* 2010; 16:541–553. [PubMed: 20068104]
19. Schwartz EL. Antivascular actions of microtubule-binding drugs. *Clin Cancer Res.* 2009; 15:2594–601. [PubMed: 19351751]
20. Wong RJ, Patel SG, Kim S, DeMatteo RP, Malhotra S, Bennett JJ, St-Louis M, Shah JP, Johnson PA, Fong Y. Cytokine gene transfer enhances herpes oncolytic therapy in murine squamous cell carcinoma. *Hum Gene Ther.* 2001; 12:253–265. [PubMed: 11177562]
21. Meignier B, Longnecker R, Roizman B. In vivo behavior of genetically engineered herpes simplex viruses R7017 and R7020: construction and evaluation in rodents. *J Infect Dis.* 1988; 158:602–14. [PubMed: 2842408]
22. Chou TC, Talalay P. Quantitative analysis of dose-effect relationships: the combined effects of multiple drugs or enzyme inhibitors. *Adv Enzyme Regul.* 1984; 22:27–55. [PubMed: 6382953]
23. Passer BJ, Wu C-I, S Wu C-I, Rabkin SD, Martuza RL. Analysis of genetically engineered oncolytic herpes simplex viruses in human prostate cancer organotypic cultures. *Gene Ther.* 2009; 16:1477–1482. [PubMed: 19693098]
24. Kanthou C, Tozer GM. Tumour targeting by microtubule-depolymerizing vascular disrupting agents. *Expert Opin Ther Targets.* 2007; 11:1443–1457. [PubMed: 18028009]
25. Folkman J. Anti-angiogenesis: new concept for therapy of solid tumors. *Ann Surg.* 1972; 175:409–416. [PubMed: 5077799]
26. Hanahan D, Weinberg RA. Hallmarks of cancer: the next generation. *Cell.* 2011; 144:646–674. [PubMed: 21376230]
27. Folkman J. Angiogenesis: an organizing principle for drug discovery? *Nat Rev Drug Discov.* 2007; 6:273–286. [PubMed: 17396134]
28. Klement G, Baruchel S, Rak J, Man S, Clark K, Hicklin DJ, Bohlen P, Kerbel RS. Continuous low-dose therapy with vinblastine and VEGF receptor-2 antibody induces sustained tumor regression without overt toxicity. *J Clin Invest.* 2000; 105:R15–24. [PubMed: 10772661]
29. Liu R, Varghese S, Rabkin SD. Oncolytic herpes simplex virus vector therapy of breast cancer in C3(1)/SV40 T-antigen transgenic mice. *Cancer Res.* 2005; 65:1532–1540. [PubMed: 15735042]
30. Liu TC, Zhang T, Fukuhara H, Kuroda T, Todo T, Canron X, Bikfalvi A, Martuza RL, Kurtz A, Rabkin SD. Dominant-negative fibroblast growth factor receptor expression enhances antitumoral

- potency of oncolytic herpes simplex virus in neural tumors. *Clin Cancer Res.* 2006; 12:6791–6799. [PubMed: 17121900]
31. Liu TC, Zhang T, Fukuhara H, Kuroda T, Todo T, Martuza RL, Kurtz A, Rabkin SD. Oncolytic HSV armed with platelet factor 4, an antiangiogenic agent, shows enhanced efficacy. *MolTher.* 2006; 14:789–797.
 32. Zhang W, Fulci G, Buhrman JS, Stemmer-Rachamimov AO, Chen JW, Wojtkiewicz GR, Weissleder R, Rabkin SD, Martuza RL. Bevacizumab With Angiostatin-armed oHSV Increases Antiangiogenesis and Decreases Bevacizumab-induced Invasion in U87 Glioma. *MolTher.* 2012; 1:37–45.
 33. Colombo MP, Trinchieri G. Interleukin-12 in anti-tumor immunity and immunotherapy. *Cytokine Growth Factor Rev.* 2002; 13:155–168. [PubMed: 11900991]
 34. Voest EE, Kenyon BM, O'Reilly MS, Truitt G, D'amato RJ, Folkman J. Inhibition of Angiogenesis In Vivo by Interleukin 12. *JNCI.* 1995; 87:581–586. [PubMed: 7538593]
 35. Yao L, Sgadari C, Furuke K, Bloom ET, Teruya-Feldstein J, Tosato G. Contribution of natural killer cells to inhibition of angiogenesis by interleukin-12. *Blood.* 1999; 5:1612–1621. [PubMed: 10029590]
 36. Yu DC, Chen Y, Dille J, Li Y, Embry M, Zhang H, Nguyen N, Amin P, Oh J, Henderson DR. Antitumor synergy of CV787, a prostate cancer-specific adenovirus, and paclitaxel and docetaxel. *Cancer Res.* 2001; 61:517–525. [PubMed: 11212244]
 37. Penfold MET, Armati P, Cunningham AL. Axonal transport of herpes simplex virions to epidermal cells: Evidence for a specialized mode of virus transport and assembly. *Proc Natl Acad Sci USA.* 91:6529–6533. [PubMed: 7517552]
 38. Avitabile E, Di Gaeta S, Torrisi MA, Ward PL, Roizman B, Campadelli-Fiume G. Redistribution of microtubules and golgi apparatus in herpes simplex virus-infected cells and their role in viral exocytosis. *J Virol.* 1995; 69:7472–782. [PubMed: 7494253]
 39. Kotaskis A, Pomeranz LE, Blouin A, Blaho JA. Microtubule reorganization during herpes simplex virus type I infection facilitates nuclear localization of VP22, a major virion tegment protein. *J Virol.* 2001; 75:8697–8711. [PubMed: 11507215]
 40. Lin S-F, Gao SP, Price DL, Li S, Chou T-C, Singh P, Huang Y-Y, Fong Y, Wong RJ. Synergy of a Herpes Oncolytic Virus and Paclitaxel for Anaplastic Thyroid Cancer. *Clin Cancer Res.* 2008; 14:1519–1528. [PubMed: 18316577]
 41. Weidner N, Carroll PR, Flax J, Blumenfeld W, Folkman J. Tumor angiogenesis correlates with metastasis in invasive prostate carcinoma. *Am J Pathol.* 1993; 143:401–409. [PubMed: 7688183]
 42. Gettman MT, Pacelli A, Slezak J, Bergstralh EJ, Blute M, Zincke H, Bostwick DG. Role of microvessel density in predicting recurrence in pathologic Stage T3 prostatic adenocarcinoma. *Urology.* 1999; 54:479–485. [PubMed: 10475358]
 43. Kelly WK, Halabi S, Carducci M, George D, Mahoney JF, Stadler WM, Morris M, Kantoff P, Monk JP, Kaplan E, Vogelzang NJ, Small EJ. Randomized, Double-Blind, Placebo-Controlled Phase III Trial Comparing Docetaxel and Prednisone With or Without Bevacizumab in Men With Metastatic Castration-Resistant Prostate Cancer: CALGB 90401. *J Clin Oncol.* 2012; 30:1534–1540. [PubMed: 22454414]
 44. Kerbel RS, Yu J, Tran J, Man S, Vilorio-Petit A, Klement G, Coomber BL, Rak J. Possible mechanisms of acquired resistance to anti-angiogenic drugs: implications for the use of combination therapy approaches. *Cancer Metastasis Rev.* 2001; 20:79–86. [PubMed: 11831651]

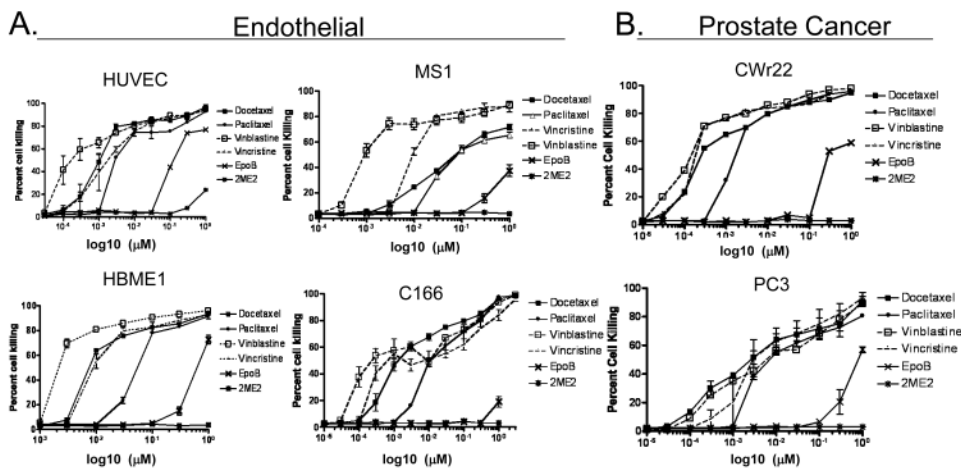


Figure 1. Cytotoxic effects of MDA's. (A) HUVEC (human umbilical vein endothelial cells) primary cultures and endothelial cell lines MS1 (mouse pancreatic), C166 (mouse yolk sac), HBME-1 (human bone marrow) and (B) Human CWR22 and PC3 prostate cancer cell lines were treated with increasing concentrations of the indicated MDA's. MTS assays were performed on day 3 to determine the extent of cell killing.

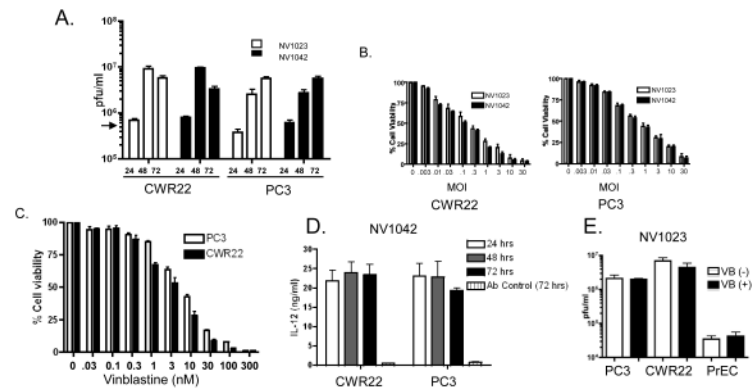


Figure 2.

Analysis of NV1023 and NV1042 replication and effects on prostate cancer cell killing (A) Single burst assays were performed using either NV1023 or NV1042 (MOI=1.5) on CWR22 or PC3 cells over a 72 hr period. Virus (cell pellet plus supernatants) on days 1, 2 and 3 post-infection and viral titers (pfu/ml) determined by plaque assay on Vero cells as described previously¹³. Input virus: $\sim 4 \times 10^5$ plaque forming units (pfu; indicated by arrow). (B) Cell susceptibility assays were performed using NV1023 or NV1042 on either CWR22 (*left*) or PC3 (*right*) prostate cancer cells. Cell lines were inoculated with the indicated MOI's of virus and cell killing was evaluated by MTS assay on day 3 (error bars represent S.E.M.). (C) PC3 (open bar) or CWR22 (solid bar) prostate cancer cells were treated with increasing concentration of VB (0.01-100 nM) and MTS assays were performed to generate dose-response curves. (D) Supernatants collected from single burst assays were assayed for IL-12 derived from NV1042 by ELISA at the indicated time points. NV1023 was used as a control vector to normalize for background and normal goat IgG control was also included to demonstrate specificity for murine IL-12. (E) Prostate cancer (PC3 and CWR22) and normal prostate epithelial (PrEC) cells were incubated in the presence or absence of non-toxic concentrations of VB (0.1 nM) for 12h and thereafter, cells were infected with NV1023 (MOI of 1.5) for 72 hrs. Virus titers were determined by plaque assay on Vero cells. Note that virus replication is not altered in the presence of VB and is negligible in PrEC.

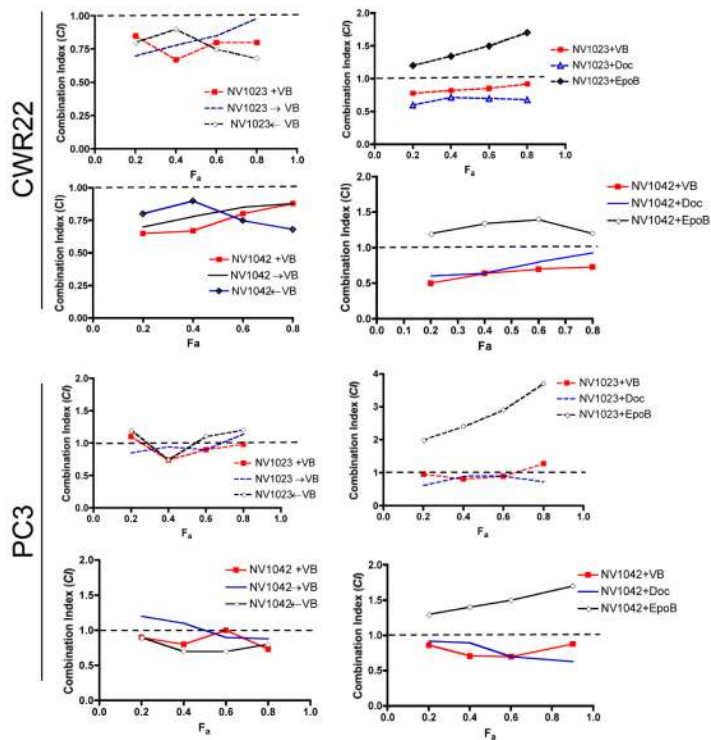


Figure 3. Combination-Index analysis. Fraction affected (F_a) versus combination index plots were generated using the method of Chou and Talalay²² to determine the extent of synergy if any for either vinblastine (VB), docetaxel (Doc) or epothilone-B (EpoB) in combination with NV1023 or NV1042 in CWR22 (*upper panels*) and PC3 (*lower panels*) cell lines. (+) indicates simultaneous oHSV and drug addition; (□) indicates oHSV inoculation 24 hrs before drug treatment; (○) indicates drug treatment 24 hrs prior to oHSV infection. Synergistic effects are defined as combination index (CI) < 1 additive effects are CI=1, and antagonistic effects are CI > 1. Note that the dotted line in each plot indicates a reference point of a CI value of 1.

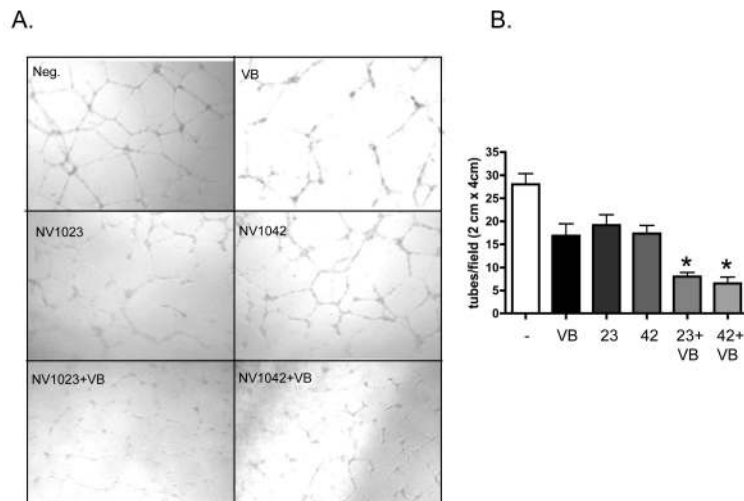
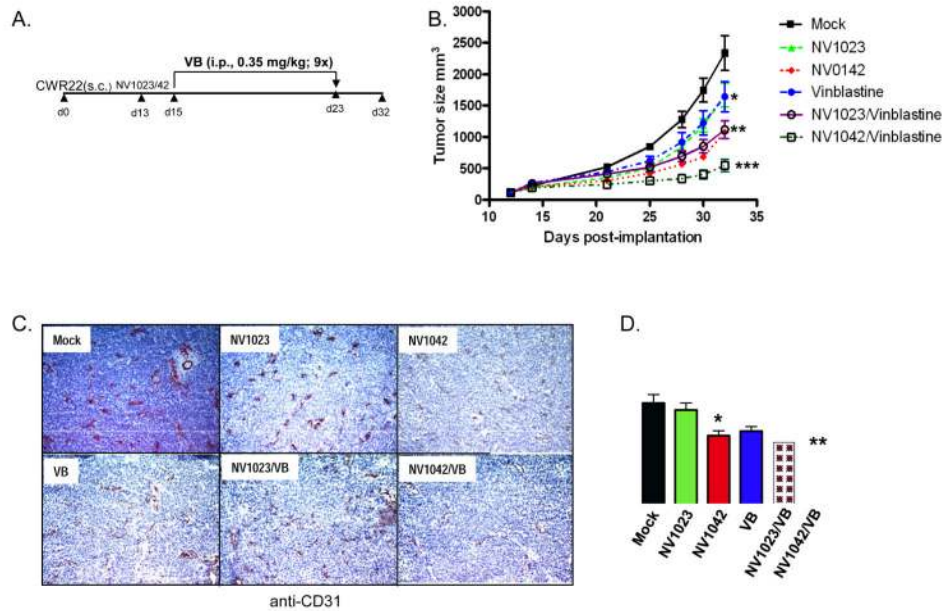


Figure 4. Increased antiangiogenic effects of NV1042/vinblastine combination in an *in vitro* tube formation assay. HUVEC cells were plated on matrigel-coated plates and either remained untreated (Neg.) or treated with NV1023 or NV1042 (MOI 1), vinblastine (1nM) or their combination. Twentyhrs later, tube formation was scored. Representative fields are shown for each condition (A) and the number of tubes/field was quantified (B). Each treatment was performed in triplicate. Student's t test was used to determine statistical significance between the indicated control and treatment groups. Bars represent average \pm S.E.M..*, $P < 0.01$ for NV1023+VB and NV1042+VB versus NV1023 alone, NV1042 alone, VB alone or untreated.

**Figure 5.**

In vivo efficacy studies. (A) Schematic illustrating the dosing and scheduling of single and combination treatment regimes in mice bearing s.c. CWR22 tumors. (B) Assessment of CWR22 tumor growth. Virus [NV1023 or NV1042; 5×10^5 plaque-forming units (pfu)] or virus suspension buffer (PBS with 10% glycerol) was injected intratumorally on days 13 and 15 after tumor implantation. Vinblastine was administered intraperitoneally at 0.35 mg/kg on day 15 for nine consecutive days. *, $P < 0.05$ for mock ($n = 8$) versus NV1023 only ($n = 8$) and VB only ($n = 7$); **, $P < 0.01$ for mock versus NV1042 only ($n = 6$) and NV1023 + VB ($n = 6$); ***, $P < 0.01$ for NV1042+VB ($n = 7$) versus NV1042 only and NV1023 + VB at day 32. (C) Evaluation of CD31⁺ staining (brown) as a function of treatment condition. Mice ($n=3$ /group) were treated as described above and at day 30 post-implantation tumors were harvested, frozen and cut into tissue sections. Tissue sections were stained with a rat anti-mouse CD31 antibody and were counterstained with hematoxylin. (D) Quantification of CD31-positive staining. Tumor microvessel density was quantified for all treatment groups. Tumor microvessel density was compared between all treatment groups and untreated control group. (Mean \pm S.E.M); * $P < 0.04$ for NV1023 versus NV1042; **, $P < 0.03$ for NV1042 versus NV1042/VB.

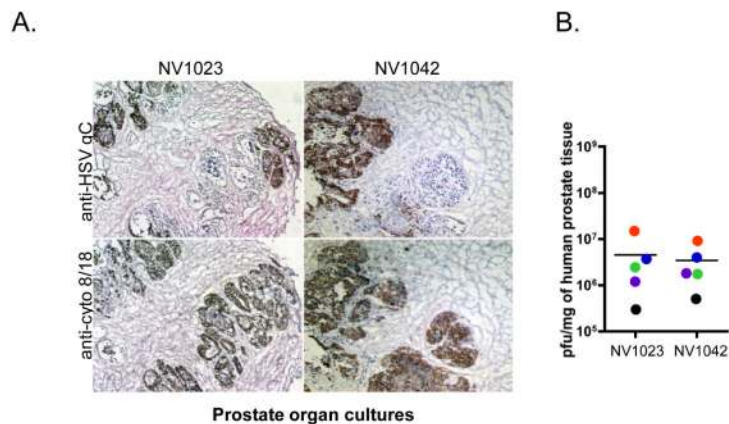


Figure 6.

Analysis of NV1023 and NV1042 infection of prostate cancer surgical samples. Tissues were incubated with NV1023 (1×10^6 pfu) or NV1042 (1×10^6 pfu) for 1 h in direct contact and thereafter, placed on a semi-submersed collagen sponge for 3 days. (A) Tissue specimens were stained with anti-HSV-1 gC (upper panels) or anti-cytokeratin-8/18 (lower panels) antibodies. Sections were counterstained with hematoxylin. Note the partial overlap between anti-HSV gC and cytokeratin-8/18⁺ staining. (B) Evaluation of NV1023 or NV1042 replication in prostate organ cultures. Each color dot indicates a different prostate surgical specimen. Horizontal line denotes the average viral titer for the two groups, which are statistically not significant. Note that infection with NV1023 or NV1042 resulted in similar viral titers. The five specimens examined represent Gleason Scores of either 3+3=6 or 3+4=7.

Table 1

	Doc	Pac	VB	VC	epoB	2ME2
HUVEC	0.88 ± 0.2	2.5 ± 1	0.18 ± 0.04	1.7 ± 0.3	540 ± 56	>1000
HBME1	7.8 ± 2	53 ± 12	1.7 ± 0.5	8.6 ± 2	540 ± 45	>1000
MS1	82 ± 11	98 ± 14	1.6 ± 0.4	8.2 ± 3	>1000	>1000
C166	1.9 ± 0.1	12 ± 4	0.38 ± 0.1	0.64 ± 0.1	>1000	>1000
CWR22	0.28 ± 0.3	1.7 ± 0.7	0.27 ± .02	0.26 ± .03	290 ± 35	>1000
Pc3	4.6 ± 0.8	6.1 ± 1	7.8 ± 1	6.3 ± 0.5	890 ± 76	>1000

Values represent EC₅₀'s; mean (nM) ±SEM; 3-day